Vacuum Polarization and Screening of Supercritical Impurities in Graphene

A. V. Shytov,[1] M. I. Katsnelson,[2] and L. S. Levitov[3]

[1]*Condensed Matter Physics and Materials Science Department, Brookhaven National Laboratory, Upton, New York 11973-5000, USA*
[2]*Radboud University of Nijmegen, Toernooiveld 1 6525 ED Nijmegen, The Netherlands*
[3]*Department of Physics, Massachusetts Institute of Technology, 77 Massachusetts Ave, Cambridge, Massachusetts 02139, USA*

(Received 31 May 2007; published 5 December 2007)

Screening of charge impurities in graphene is analyzed using the exact solution for vacuum polarization obtained from the massless Dirac-Kepler problem. For the impurity charge below a certain critical value, no density perturbation is found away from the impurity, in agreement with perturbation theory. For the supercritical charge, however, the polarization distribution is shown to have a power law profile, leading to screening of the excess charge at large distances. The Dirac-Kepler scattering states give rise to standing wave oscillations in the local density of states which are prominent in the supercritical regime.

DOI: 10.1103/PhysRevLett.99.236801 PACS numbers: 73.43.−f, 73.63.Fg, 81.05.Uw

Massless Dirac excitations in graphene [1] provide an interesting realization of quantum electrodynamics (QED) in dimension two [2]. Because of a zero mass and strong interactions, characterized by a large "fine structure constant" $\alpha = e^2/\hbar v_F \approx 2.5$, where $v_F \approx 10^6$ m/s is the Fermi velocity, this material breaks away from the perturbative QED paradigm. One of the phenomena fundamental in QED, expected to become strong in graphene, is "vacuum polarization" induced by charge impurities. Although the problem of Coulomb scattering received a lot of attention [3–8], the key question of screening of the impurity potential outside the weak coupling regime has not been adequately addressed [7,8].

Here, we present an accurate nonperturbative treatment of this problem based on the vacuum polarization found from the exact solution of the $2d$ Dirac-Kepler problem. There are two qualitatively different regimes emerging from this solution, which are somewhat analogous to those known in QED of heavy atoms [9]. The Dirac equation with a Coulomb-like singularity is consistent only for a potential of a subcritical strength while in the supercritical case a finite nuclear radius must be accounted for [10]. We shall see that a similar behavior arises in our problem above the critical charge value

$$\beta = \beta_c = \frac{1}{2}, \qquad \beta \equiv \frac{Ze^2}{\kappa\hbar v_F}, \tag{1}$$

where κ is the effective dielectric constant. For the case when screening is solely due to the graphene electrons, the RPA approach [2] gives $\kappa_{\mathrm{RPA}} \approx 5$. With $e^2/\hbar v_F \approx 2.5$, this yields a critical value $Z_c \approx 1$.

The most prominent effect in our problem, arising at supercritical β, is the change in the character of polarization of the Dirac vacuum. While at $\beta < \frac{1}{2}$ the polarization charge q_p is localized on the scale of the impurity radius and exhibits no long range tail [8], for supercritical β, our solution of the massless Dirac equation for noninteracting fermions predicts polarization of a power law form. For $\frac{1}{2} < \beta < \frac{3}{2}$, when just the lowest angular momentum channels are overcritical, we find

$$n_{\mathrm{pol}}(\rho) \approx -\frac{N\gamma \mathrm{sgn}\beta}{2\pi^2\rho^2} - q_p\delta(\rho), \quad \gamma \equiv \sqrt{\beta^2 - 1/4}, \tag{2}$$

where $N = 4$ is the combined spin and valley degeneracy of graphene. At higher β, the polarization charge still exhibits a tail of a $1/\rho^2$ form [see Eq. (27)].

The result (2), found for noninteracting fermions, can be used to describe screening in an interacting system in a self-consistent renormalization group (RG) fashion. The RG flow for a polarized cloud is constructed by proceeding from the lattice scale $\rho = r_0$ to larger ρ, treating the net polarization charge with the radius ρ as an effective point charge $\beta(\rho)$, and using it to determine polarization at distances $\rho' > \rho$. As a result, the net charge $\beta(\rho)$ flows from its initial value $\beta(r_0)$ to lower values. The net charge (2) within the annulus $\rho_1 < \rho < \rho_2$ equals $\delta Z = -N\mathrm{sgn}\beta\frac{\gamma}{\pi}\ln(\rho_2/\rho_1)$, which gives an RG equation

$$\frac{d\beta(\rho)}{d\ln\rho} = -\frac{Ne^2\mathrm{sgn}\beta}{\pi\kappa\hbar v_F}\gamma(\rho), \qquad \beta > \beta_c. \tag{3}$$

Integrating the flow (3), we find that it terminates at a distance $\rho_* = r_0\exp[\frac{\pi\kappa\hbar v_F}{Ne^2}\cosh^{-1}(2\beta)]$ where β reaches the critical value (1). In contrast to screening in metals, here the polarization buildup brings the net charge down to the critical value β_c that remains unscreened at larger distances $\rho \gtrsim \rho_*$. The RG treatment is applicable when the RG flow is slow, i.e., when the right-hand side of Eq. (3) is small. Thus, the RG framework is adequate near the criticality, $\beta \approx \beta_c$, where γ is small, even in the case of strong coupling, $e^2/\kappa\hbar v_F \sim 1$, and the predicted termination of screening at large ρ is universal.

Our treatment of vacuum polarization relies on the exact solution of the Dirac-Kepler problem from which we extract scattering phases and use them in the Friedel sum rule framework to evaluate the screening charge. The phases are found to behave differently for $\beta < \beta_c$ and $\beta > \beta_c$. In the first case, the essential part of the phase is $\beta\ln k\rho$, while in the second case, it is $\beta\ln k\rho - \gamma\mathrm{sgn}\beta\ln kr_0$. Notably,

the term $\beta \ln k\rho$ is the same for all angular momentum channels. Such a contribution to the phase, as Ref. [11] insightfully remarks, arises from quasiclassical dynamics at large distances and has nothing to do with scattering. Accordingly, we find that it does not affect polarization at finite ρ, while the term $-\gamma \mathrm{sgn}\beta \ln k r_0$ gives rise to the power law in (2).

Now we turn to the analysis of the massless Dirac equation in dimension two in a central potential $V(\rho)$:

$$\hbar v_F \begin{pmatrix} 0 & -i\partial_x - \partial_y \\ -i\partial_x + \partial_y & 0 \end{pmatrix} \psi = [\varepsilon - V(\rho)]\psi. \quad (4)$$

Introducing polar coordinates $x + iy = \rho e^{i\varphi}$, we separate angular harmonics of the two-component wave function ψ and seek the solution in the form [12]

$$\psi(\rho, \varphi) = \begin{pmatrix} w(\rho) + v(\rho) \\ [w(\rho) - v(\rho)]e^{i\varphi} \end{pmatrix} \rho^{s-1/2} e^{i(m-1/2)\varphi} e^{ik\rho}, \quad (5)$$

with *halfinteger* angular quantum number m. The terms w and v represent the incoming and outgoing waves. The parameters s and k are determined by the behavior at small and large ρ. For $V(\rho) = Ze^2/\rho$, we find

$$s = \sqrt{m^2 - \beta^2}, \qquad k = -\frac{\varepsilon}{\hbar v_F}, \quad (6)$$

where β is the dimensionless coupling (1). [The minus sign in (6) is chosen to make $k > 0$ in the Fermi sea.] The solution (5) behaves differently for $|\beta| < |m|$, when the exponent s is real, and $|\beta| > |m|$, when s becomes complex imaginary.

The ansatz (5), substituted into Dirac equation, yields coupled equations for the functions $w(\rho)$ and $v(\rho)$:

$$\rho \partial_\rho w + (s + i\beta + 2ik\rho)w - mv = 0, \quad (7)$$

$$\rho \partial_\rho v + (s - i\beta)v - mw = 0. \quad (8)$$

We eliminate w and introduce a new independent variable $z = -2ik\rho$ to obtain a hypergeometric equation

$$zv'' + (2s + 1 - z)v' - (s - i\beta)v = 0. \quad (9)$$

The solution regular at $z = 0$ is given by the confluent hypergeometric function [13]:

$$v(z) = A_1 F_1(s - i\beta, 2s + 1, z), \quad (10)$$

$$w(z) = A \frac{s - i\beta}{m} {}_1F_1(s + 1 - i\beta, 2s + 1, z), \quad (11)$$

where A is a normalization factor. The expression for w was obtained using Eq. (8) and an identity for ${}_1F_1$ [14].

The solution (5), (10), and (11) of the Dirac-Kepler problem, regular at $\rho = 0$, can be used to evaluate the polarization charge in the subcritical case $|\beta| < 1/2$. This can be done most easily using the scattering phases, given by the behavior of w and v at large ρ. Using the asymptotic form of the functions ${}_1F_1$ [15], we find

$$v(\rho) = \frac{\lambda e^{i\beta \ln(2k\rho)}}{(2k\rho)^s}, \qquad w(\rho) = \frac{\lambda^* e^{-i\beta \ln(2k\rho)} e^{-2ik\rho}}{(2k\rho)^s}, \quad (12)$$

where the parameter λ depends on m and β but not on k. From (12), we see that $\rho^{s-(1/2)} w(\rho) \exp(ik\rho)$ and $\rho^{s-(1/2)} v(\rho) \exp(ik\rho)$ indeed describe the incoming and the outgoing waves, characterized by relative phase

$$v/w = e^{2i\delta_m(k) + 2ik\rho}, \qquad \delta_m(k) = \beta \ln(2k\rho) + \arg\lambda. \quad (13)$$

The log dependence in Eq. (13) is typical for the phase coming from $1/r$ Coulomb tail [11].

The scattering phases $\delta_m(k)$ can be used to find the polarization charge pulled on the origin. However, a straightforward application of the Friedel sum rule [16,17], involving phases evaluated at the Fermi level, encounters a difficulty due to the position and energy dependence of the phases in Eq. (13). Since this may indicate that the polarization is distributed rather than localized at $\rho = 0$, we proceed with caution.

To evaluate the excess particle number $Q_{\mathrm{pol}}(\rho)$ in the region $0 \le \rho' < \rho$, we note that the states with $|k| \lesssim 1/\rho$, i.e., of wavelength in excess of ρ, contribute negligibly to $Q_{\mathrm{pol}}(\rho)$. Thus, we can write the sum rule [16,17] as

$$Q_{\mathrm{pol}}(\rho) \approx -\frac{N}{\pi} \sum_m \delta_m(k \sim 1/\rho), \quad (14)$$

where the minus sign corresponds to that in Eq. (6). Conveniently, the expressions (13) for $\delta_m(k)$, valid at $k\rho \gtrsim 1$, can be used to evaluate (14). However, since $\delta_m(k)$ depend on the product $k\rho$, they yield a ρ-independent result for $Q_{\mathrm{pol}}(\rho)$. We therefore conclude that the polarization charge is concentrated on the lattice scale $\rho \approx r_0$.

To independently verify the conclusion about polarization at $\beta < 1/2$ concentrated at $\rho \lesssim r_0$, we evaluated it directly using the eigenstates given by Eqs. (5), (10), and (11). This calculation involves an energy cutoff introduced at the bottom of graphene band, corresponding to $k \approx r_0^{-1}$. We found nonvanishing contribution to polarization charge only on the cutoff scale, leading to an expression $n_{\mathrm{pol}}(\rho) = -q_p \delta(\rho)$ [the second term in Eq. (2)]. This form of polarization charge can be independently justified by the RPA method [4,8], giving $q_p = \frac{\pi}{2}\beta$. Our numerical results at $0 < |\beta| \lesssim 1$, presented in Fig. 1, yield a similar dependence, nearly linear at $|\beta| < \frac{1}{2}$, independently confirming the above analysis.

The behavior of the scattering phase and of the polarization charge changes when the potential strength $|\beta|$ exceeds $|m|$ for one or several values of m. For such supercritical β, Eq. (10) is not the only possible solution. Adding another solution of the Eq. (9), we write the function $v(z)$ in the form

$$v(z) = A_1 F_1(i(\gamma - \beta), 1 + 2i\gamma, z) + B z_1^{-2i\gamma} F_1(-i(\gamma + \beta), 1 - 2i\gamma, z), \quad (15)$$

where $\gamma = \mathrm{Im} s = \sqrt{\beta^2 - m^2}$, and $z = -2ik\rho$. With the help of the relation [14], we find

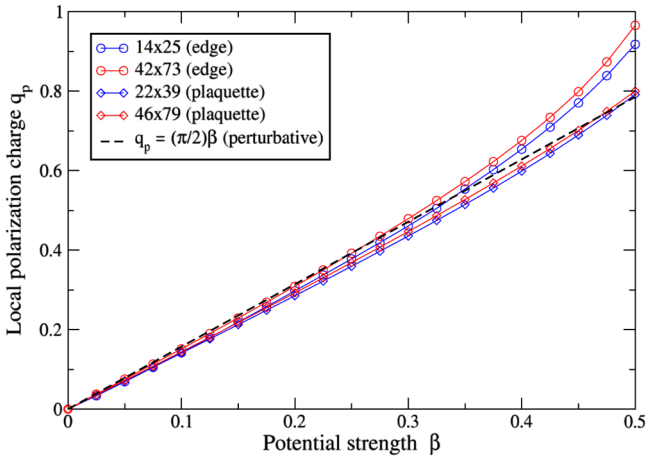

FIG. 1 (color online). Local polarization charge found from numerical solution of a tight-binding problem on a honeycomb lattice. The charge was placed in the middle of a rectangular region of size $n_1 \times n_2$ at the lattice plaquette center or edge center (see legend). Shown is the net polarization at a distance of less than 5 lattice constants from point charge, which agrees with the prediction of a perturbative RPA calculation (dashed line).

$$w(z) = -iA\eta\, {}_1F_1(1 + i\gamma - i\beta, 1 + 2i\gamma, z) - i(B/\eta) z^{-2i\gamma}\, {}_1F_1(1 - i\gamma - i\beta, 1 - 2i\gamma, z), \quad (16)$$

where $\eta = \beta - \gamma/\beta + \gamma$.

To find the relation between A and B, we consider our solution at small distances, $\rho \approx r_0 \ll 1/k$:

$$v(\rho) \approx A + Be^{-\pi\gamma} e^{-2i\gamma \ln(2k\rho)}, \quad (17)$$

$$w(\rho) \approx -iA\eta - i(B/\eta) e^{-\pi\gamma} e^{-2i\gamma \ln(2k\rho)}. \quad (18)$$

Motivated by the description of zigzag edge [18], and without loss of generality, we use the boundary condition $\psi_2(\rho = r_0) = 0$ for the wave function (5), which enforces zero amplitude on one of the graphene lattice sites. Solving the equation $v(r_0) = w(r_0)$, we find the relation

$$B = e^{2i\chi(k)} \eta e^{\pi\gamma} A, \quad e^{2i\chi(k)} = -i\frac{1 - i\eta}{1 + i\eta} e^{2i\gamma \ln 2kr_0}. \quad (19)$$

The product kr_0 is very small for typical k, making the phase factor $e^{2i\chi(k)}$ a rapidly oscillating function of k.

To better understand the role of the second solution, let us take another look at the subcritical case, $|\beta| < |m|$, when the parameter s, Eq. (6), is real. In this case, two independent solutions are still provided by Eqs. (15) and (16), whereby $i\gamma$ is replaced by s. Applying the boundary conditions the same way as above, instead of (19), we find $B/A \propto (2kr_0)^{2s} \ll 1$, which indicates that the second solution plays no role in the subcritical case.

To link $\chi(k)$, Eq. (19), to the scattering phase, we write our solution for $v(\rho)$, $w(\rho)$ at large distances $\rho k \gg 1$, again using the asymptotic expression for ${}_1F_1$ [15],

$$\frac{v}{w} = \frac{g_{\beta,\gamma} + e^{2i\chi} e^{-\pi\gamma} \eta g_{\beta,-\gamma}}{e^{-\pi\gamma} \eta g^*_{\beta,-\gamma} + e^{2i\chi} g^*_{\beta,\gamma}} e^{2ik\rho} e^{2i\beta \ln 2k\rho}, \quad (20)$$

where $g_{\beta,\gamma} = \Gamma(1 + 2i\gamma)/\Gamma(1 + i\gamma + i\beta)$. We note that (20) automatically satisfies the current conservation requirement $|v| = |w|$. The relative phase of v and w, defined as in Eq. (13), thus equals

$$\delta_m(k) = \theta(k) + \beta \ln 2k\rho + \arg g_{\beta,\gamma}, \quad (21)$$

where

$$\theta(k) = \arg[e^{-i\chi(k)} + ae^{i\chi(k)}], \quad a = e^{-\pi\gamma} \eta \frac{g_{\beta,-\gamma}}{g_{\beta,\gamma}}. \quad (22)$$

The last two terms of the phase (21) are identical in form to (13). They represent spherical wave "deformed" by the tail of Coulomb potential at large distances and, as we discussed above, give no contribution to polarization charge at finite ρ. The term $\theta(k)$, however, arising from the boundary condition at small ρ via the phase $\chi = \arg(B/A)$, Eq. (19), makes the behavior completely different from that found for $|\beta| < |m|$.

The phase $\theta(k)$ dependence on k is determined by the relation between θ and χ, Eq. (22). For the latter, the winding number depends on

$$|a| = \sqrt{\frac{e^{-2\pi\gamma} - e^{-2\pi\beta}}{e^{2\pi\gamma} - e^{-2\pi\beta}}} = \begin{cases} <1 & \text{if } \beta > 0, \\ >1 & \text{if } \beta < 0. \end{cases} \quad (23)$$

(We recall that $0 < \gamma < |\beta|$.) The phase θ winding is thus controlled by the first term of (22) at $\beta > 0$ and by the second term at $\beta < 0$, allowing us to write it as

$$\theta(k) = -\mathrm{sgn}\beta\, \chi(k) + \Delta\theta(k), \quad (24)$$

where $\Delta\theta$ is an oscillatory periodic function of χ.

It is instructive to compare the behavior of $\Delta\theta(k)$ at strongly overcritical and nearly critical β. For large $|\beta|$, we have $\gamma \approx |\beta|$ and $|a| \approx e^{-2\pi\gamma}$, and thus $\Delta\theta$ is exponentially small. In the opposite limit of nearly critical $\beta \approx \beta_c = \pm m$, we expand $|a|$ in small γ to find $|a| = 1 - O(\gamma)$. In this case, θ, as a function of χ, is a staircase with steps of height π, width π, and corners rounded on the scale $O(\gamma)$. The staircase slope $-\frac{1}{2}\mathrm{sgn}\beta$ corresponds to the first term in Eq. (24). The oscillatory part $\Delta\theta(k)$ manifests itself in the local density of states around the impurity (see peak in the $\varepsilon < 0$ region in Fig. 2 inset).

To analyze the contribution of the phase $\theta(k)$ to the polarization density, we suppress the periodic part $\Delta\theta$. Using the expression (22), we find $\theta(k) = -\gamma \mathrm{sgn}\beta \ln 2kr_0$. Substituting it in the Friedel sum rule, Eq. (14), we find

$$Q_{\mathrm{pol}}(\rho) = -N\frac{\theta(k \sim 1/\rho)}{\pi} = -\mathrm{sgn}\beta \frac{\gamma N}{\pi} \ln\frac{\rho}{2r_0}. \quad (25)$$

From $n_{\mathrm{pol}}(\rho) = (2\pi\rho)^{-1} dQ_{\mathrm{pol}}/d\rho$, we find the polarization density (2). When the parameter s is complex in more than one channel, one has to consider a sum

$$n_{\mathrm{pol}}(\rho) = -\frac{N\mathrm{sgn}\beta}{2\pi^2\rho^2} \sum_{|m|<|\beta|} \sqrt{\beta^2 - m^2}. \quad (26)$$

For large $\beta \gg 1$, replacing the sum by an integral, we re-

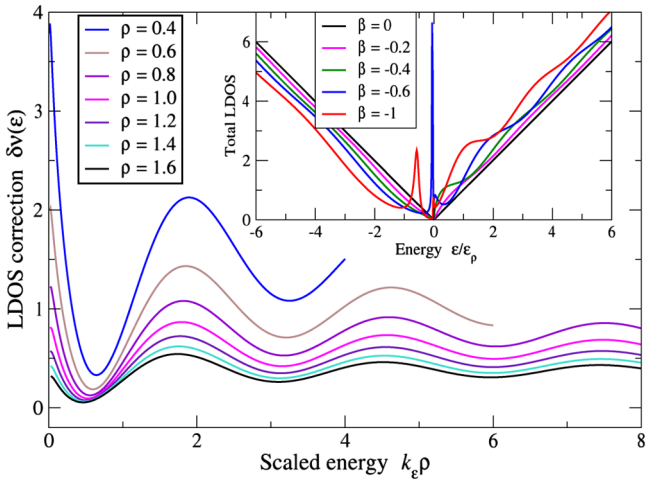

FIG. 2 (color online). Standing wave oscillations in LDOS, Eq. (27), vs. energy scaled by the distance from impurity ρ. Maxima (minima) occur at half-integer (integer) values of $k\rho/\pi$. LDOS is shown for an overcritical $\beta = 0.6$ and several values of ρ, given in the units of $10^3 r_0$. *Inset:* Oscillations in LDOS, appearing for $|\beta| > \frac{1}{2}$ on the top of the unperturbed density of states, which is subtracted in the main figure ($\varepsilon_\rho = \hbar v_F/\rho$).

cover the Thomas-Fermi result $n_{\rm pol}(\rho) = N\beta|\beta|/(4\pi\rho^2)$ found in [7] for noninteracting fermions.

For supercritical $\beta > \frac{1}{2}$, as discussed above, the scattering phase becomes sensitive to the physics at small distances, $\rho \approx r_0$. This leads to pronounced interference of the incoming and outgoing waves, which is manifest in the local density of states (LDOS),

$$\nu(\varepsilon, \rho) = \frac{N}{\pi\hbar v_F}\sum_m |\psi(k_\varepsilon, \rho)|^2, \qquad k_\varepsilon = -\frac{\varepsilon}{\hbar v_F}, \quad (27)$$

with an appropriate normalization of the two-component wave function ψ, Eq. (5). We evaluated the sum in (27) numerically, using the expressions (15) and (16). For $0 < |\beta| < \frac{1}{2}$, LDOS does not deviate too much from $\nu_{\beta=0} \propto |\varepsilon|$ (see Fig. 2 inset). For supercritical β, however, LDOS develops pronounced oscillations in both position ρ and energy k_ε. The crossover from a nonoscillatory to oscillatory behavior at $\beta \approx \frac{1}{2}$ becomes sharp at $\rho \gg r_0$.

The standing waves in LDOS (27) at $\beta > \frac{1}{2}$ are different from Friedel oscillations, since $k_F = 0$ for the Fermi level centered at the Dirac point: the spatial period scales inversely with energy, so that the maxima occur at $k_\varepsilon\rho = (n + \frac{1}{2})\pi$ (see Fig. 2). This is similar to the oscillations in LDOS studied in carbon nanotubes [19]. As in Ref. [19], the energy-dependent spatial period can be used to obtain direct information about Fermi velocity v_F in graphene.

Spatial periodicity of this modulation and its energy dependence are purely geometric and thus do not depend on the impurity charge. However, as Fig. 2 demonstrates, the modulation remains weak for subcritical charge and becomes strong for supercritical impurities. Thus, in the interacting case, it will extend up to the vacuum polarization cloud radius ρ_*. At such distances, it will be affected by finite temperature $T \gtrsim T_* = \hbar v_F/\rho_*$, and also by carrier doping away from neutrality by $\delta n \gtrsim \rho_*^{-2}$ strong enough to induce screening at distances less than ρ_*.

To summarize, we found that the excess charge $\beta - \frac{1}{2}$ of supercritical impurities in graphene is fully screened by the Dirac vacuum polarization. The large screening cloud size and the standing wave oscillations predicted within it can be directly probed by STM technique. The sharp departure from linear screening for supercritical impurities represents an interesting example of nonlinear screening that can be realized in graphene. Our estimates for the critical charge, using $\kappa_{\rm RPA} \approx 5$, yield an experimentally convenient value $Z_c \sim 1$, making experimental tests of these effects in graphene practical.

This work is supported by the DOE (Contract No. DEAC 02-98 CH 10886), FOM (The Netherlands), NSF MRSEC (No. DMR 02132802) and No. NSF-NIRT DMR-0304019.

[1] A. K. Geim and K. S. Novoselov, Nat. Mater. **6**, 183 (2007).
[2] J. González, F. Guinea, and M. A. H. Vozmediano, Nucl. Phys. B **424**, 595 (1994); J. Low Temp. Phys. **99**, 287 (1995).
[3] K. Nomura and A. H. MacDonald, Phys. Rev. Lett. **96**, 256602 (2006).
[4] T. Ando, J. Phys. Soc. Jpn. **75**, 074716 (2006).
[5] E. H. Hwang, S. Adam, and S. Das Sarma, Phys. Rev. Lett. **98**, 186806 (2007).
[6] D. P. DiVincenzo and E. J. Mele, Phys. Rev. B **29**, 1685 (1984).
[7] M. I. Katsnelson, Phys. Rev. B **74**, 201401(R) (2006).
[8] P. M. Ostrovsky, I. V. Gornyi, and A. D. Mirlin, Phys. Rev. B **74**, 235443 (2006).
[9] Y. B. Zeldovich and V. S. Popov, Usp. Fiz. Nauk **105**, 403 (1971); Sov. Phys. Usp. **14**, 673 (1972).
[10] I. Pomeranchuk and Y. Smorodinsky, J. Phys. (Moscow) **9**, 97 (1945).
[11] L. D. Landau and E. M. Lifshitz, *Quantum Mechanics* (Pergamon, London, 1977), 3rd ed., Chap. XVII, § 135.
[12] We use the ansatz $\psi \propto \rho^{s-1/2}$, as appropriate for the $2d$ case, instead of $\psi \propto \rho^{s-1}$, which is a convention in $3d$.
[13] M. Abramowitz and I. A. Stegun, *Handbook of Mathematical Functions* (Dover, New York, 1964).
[14] $z_1 F_1'(\alpha, \gamma, z) = \alpha[{}_1F_1(\alpha + 1, \gamma, z) - {}_1F_1(\alpha, \gamma, z)]$, which follows from Eqs. (13.4.8), (13.4.4) of Ref. [13].
[15] ${}_1F_1(a, c; z) \approx \frac{\Gamma(c)}{\Gamma(c-a)}(-z)^{-a} + \frac{\Gamma(c)}{\Gamma(a)}e^z z^{a-c}$ for large $|z|$ (see Eq. (13.5.1), Ref. [13]).
[16] J. Friedel, Philos. Mag. **43**, 153 (1952).
[17] D.-H. Lin, Phys. Rev. A **72**, 012701 (2005); **73**, 052113 (2006).
[18] D. A. Abanin, P. A. Lee, and L. S. Levitov, Solid State Commun. **143**, 77 (2007).
[19] M. Ouyang, J.-L. Huang, and C. M. Lieber, Phys. Rev. Lett. **88**, 066804 (2002).